ACS OMEGA

http://pubs.acs.org/journal/acsodf

Article

Recyclable, UV-Blocking, and Radiative Cooling Multifunctional Composite Membranes

Shaofeng Liang, Muqun Wang, Wei Gao,* Hailin Diao, and Jianju Luo

Cite This: *ACS Omega* 2022, 7, 25244−25252

Read Online

ACCESS | Metrics & More | Article Recommendations | Supporting Information

ABSTRACT: It is well known that UV radiation can cause human health problems and that energy consumption can lead to human survival problems. Here, we prepared a composite membrane that can block UV radiation as well as reduce energy consumption. Carbon dots (CDs) and acrylates were prepared from xylose and epoxidized soybean oil as biomass feedstocks, respectively, and the composite membrane was prepared by a self-assembly strategy. The first layer of the membrane is composed of CDs and epoxy resin. Its main function is not only to weaken UV rays and the aggregation-induced quenching effect of CDs but also to reduce the absorption of UV rays by the second layer of the membrane. The second layer consists of barium sulfate ($BaSO_4$) and acrylate. Compared to TiO_2 (3.2 eV), $BaSO_4$ (~6 eV) has a higher electronic band gap, which reduces the absorption of UV light by the membrane. The composite membrane exhibits excellent UV-blocking and radiative cooling performance, shielding 99% of UV rays. In addition, the membrane can reduce 4.4 °C in radiative cooling tests, achieving a good cooling effect. Finally, the recyclability of the $BaSO_4$/acrylate membrane is discussed, and 95% recovery rate provides sustainable utilization of the membrane. The composite membrane is expected to be popularized and used in low latitudes and areas with high temperature and high UV radiation near the equator.

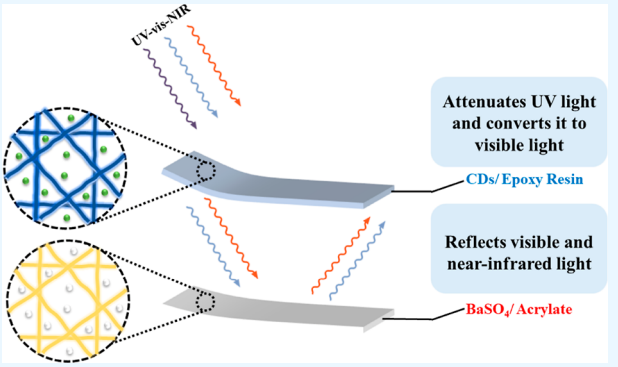

INTRODUCTION

Refrigeration is becoming increasingly important to human society due to global warming and rising living standards.[1] However, today's cooling technology is mostly dependent on energy consumption, which is only intensifying due to the increasing heat island effect in cities.[2,3] Therefore, cooling technology that achieves the purpose of cooling without consuming any energy is an urgent need in today's society.[4,5]

Radiative cooling as a passive cooling strategy with zero power consumption has shown great promise in reducing cooling costs in a variety of cooling applications.[6] Radiative cooling has become an attractive concept as it aims to solve the problems associated with energy consumption and to reduce the urban heat island effect. High-whiteness nanoparticles, such as TiO_2 and $BaSO_4$, are typical materials that impart radiative cooling properties. For example, Bao et al.[7] proposed a highly scalable nanoparticle-based double-layer coating based on TiO_2 for efficient radiative cooling. The coating is about 17 °C below ambient temperature at night and 5 °C below ambient temperature in direct sunlight. Besides, Cheng et al.[8] demonstrated a large-scale radiative cooling coating with the biomimetic structure of human skin natural wrinkle, comprising high concentrations of $BaSO_4$ particles. The maximum sub-ambient temperature drop can reach 8.1 °C. Definitely, radiative cooling has an undeniable potential for applications.[9]

Acrylate is a commonly used carrier in the study of radiative cooling membranes.[10,11] However, limited by the shortage of oil resources, unconventional oil resources derived from plants or crops have attracted great interest in academia and industry due to their biorenewable, sustainable, and environmentally-friendly characteristics.[12,13] For example, soybean oil, which is abundantly produced worldwide, is widely used in the food industry. It is formulated into epoxidized SBO (ESO), which undergoes a ring-opening reaction with acrylic acid (AA), and the obtained ESO-based epoxy acrylate is an important type of free-radical UV-curable prepolymer, which has the advantages of facile synthesis, low energy consumption, and less pollution.[14] Therefore, epoxy acrylate synthesized by using ESO is an ideal high-whiteness particle carrier in this work.

Also troublesome is the severe damage to the ozone layer due to global warming,[15] which can directly lead to an increase in the intensity of UV radiation and threaten human health. The ozone layer is able to absorb intense solar UV radiation,

Received: April 7, 2022
Accepted: June 30, 2022
Published: July 12, 2022

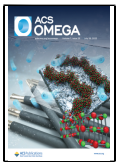

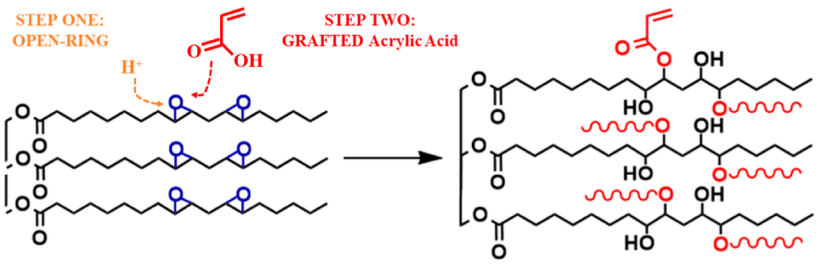

Figure 1. Synthetic principle of acrylate (the signification of the twisted red line is AA).

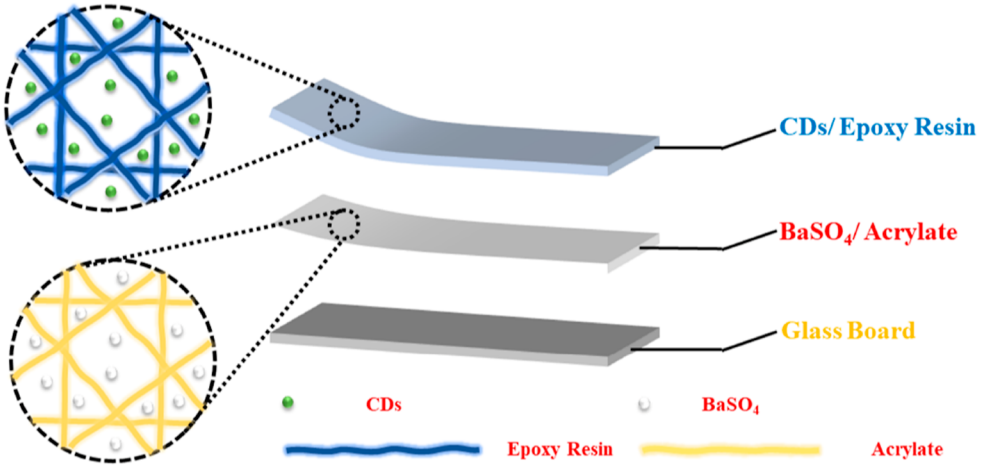

Figure 2. Synthesis of composite membranes.

but it has been decreasing.[16] Carbon dots (CDs) have a wide range of absorption properties in the UV region, which make them a promising candidate for UV-shielding materials. Importantly, CDs have demonstrated excellent UV-shielding capabilities in the existing studies.[17−19] Currently, in order to realize the large-scale and sustainable application of CDs, sustainable carbon sources are essential. Further, carbohydrates, such as xylose, are considered to be one of the most promising carbon sources due to their abundance, renewable, economical, and nontoxic properties.[20] However, to realize the widespread use of CDs, another problem needs to be solved—the aggregation-induced quenching (AIQ) effect. Fortunately, it has been found that the AIQ effect of CDs can be effectively avoided by compounding CDs with polymer matrixes.[21,22] Typically, De et al. incorporated CDs in the epoxy resin formation process to prepare a high-efficiency photoluminescent epoxy/CD nanocomposite.[23]

Above all, to cope with the energy consumption caused by cooling and the increase of UV radiation caused by global warming, the idea of designing a material that provides a cooling effect without consuming energy and that shields against UV rays is feasible because it can alleviate energy consumption, provide more time for the development of new energy, and also address the negative health effects of intense UV radiation.

In this study, we synthesized a recyclable composite membrane with radiative cooling and UV-blocking effects. First, CDs were prepared from xylose, and the first layer of the membrane was composed of CDs and epoxy resin. Then, acrylate was prepared with ESO as the raw material, and $BaSO_4$ was compounded into the acrylate to form the second membrane. Finally, they were prepared into a composite membrane by a self-assembly strategy. The composite membrane thus composed showed excellent UV-blocking ability and radiative cooling effect, and its UV-shielding rate reached 99%, almost shielding UV radiation. In indoor and outdoor tests, cooling effects of 8.4 °C and 4.4 °C were achieved, respectively. The $BaSO_4$/acrylate membrane also has a 95% recycling rate, which provides it with sustainable use.

EXPERIMENTAL SECTION

Materials. D-Xylose (98%, Macklin), *m*-phenylenediamine (99%, Macklin), ESO (Macklin), AA (99%, Aladdin), *p*-toluenesulfonic acid (99%, Macklin), hydroquinone (99%, Macklin), trimethylolpropane triacrylate (TMPTA, 95%, Macklin), 2-hydroxy-2-methylpropiophenone (I1173,97%, Macklin), and barium sulfate ($BaSO_4$, AR, Macklin) were used. Both epoxy resin and curing agent were purchased from Wenzhou Yichen Industrial Co., Ltd. All chemicals were used without further purification. A polymethyl methacrylate (PMMA) board of dimensions 20 × 20 × 0.5 cm^3 was used.

Synthesis of CDs. CDs were synthesized as follows: 0.3 g xylose with 0.15 g *m*-phenylenediamine was added to 50 mL of deionized (DI) water, fully dissolved, transferred to a microwave oven, and heated at 700 W for 15 min. After the reaction, DI water was added to redissolve, and the obtained solution was transferred to a dialysis bag (MD25-3000), and CDs were obtained after dialyzing for 3 days. The solution was freeze-dried to a powder for characterization.

Synthesis of Acrylate. The principle of acrylate synthesis is shown in Figure 1. ESO (10 g) is added to 0.32 g of *p*-toluenesulfonic acid and 0.08 g of hydroquinone and stirred at 60 °C until the solid was completely dissolved. Then, 4.32 g of AA was added, the temperature was raised to 100 °C, and heated for 3 h. After the reaction, 10 wt % TMPTA and 3 wt % I1173 were added to obtain UV-curing acrylate.

https://doi.org/10.1021/acsomega.2c02162
ACS Omega 2022, 7, 25244−25252

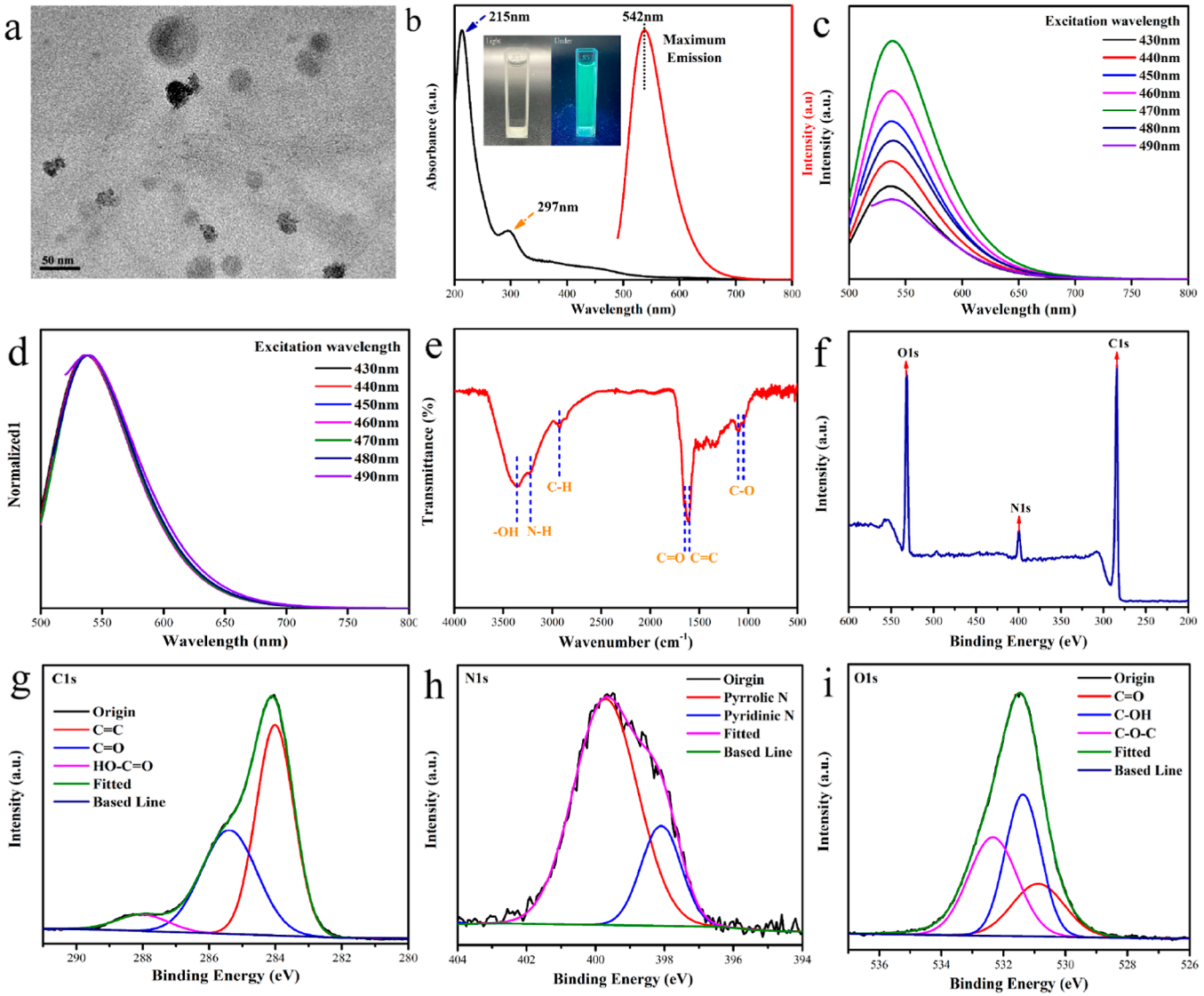

Figure 3. (a) TEM image of CDs. (b) UV−vis absorbance (left axis, black line) and fluorescence spectra (right axis, red line) [the illustration is shown before and after CDs irradiated with light (365 nm)]. (c) Different excitation wavelength (430~490 nm) fluorescence emission spectra and the (d) corresponding normalized spectra. (e) FTIR spectrum. (f) XPS spectrum. Deconvolution of XPS spectrum: (g) C 1s, (h) N 1s, and (i) O 1s.

Synthesis of Composite Membranes. The preparation of multifunctional membranes was performed by using a self-assembly method (Figure 2). Step 1: 10 g of acrylate was added to 10, 20, 30, 40, and 50% of $BaSO_4$, respectively, stirred evenly, spread evenly on a glass plate, and cured for 1 h to obtain a series of $BaSO_4$/acrylate membranes, named Mem-Ba_x (x represents the amount of $BaSO_4$ added); Step 2: 0.1 g of CDs is mixed with epoxy resin thoroughly, appropriate amount of curing agent is added and spread evenly on the $BaSO_4$/acrylate membrane, and cured for 12 h to obtain the composite membranes. The composite membranes were named Co-Mem-Ba_x (x represents the amount of $BaSO_4$ added).

Characterization. TEM of CDs was performed by a 300 kV field emission transmission electron microscope (FEI TECNAI G2 F30, FEI, USA); electron transition was performed by a UV−vis spectrophotometer (Agilent 8453, Agilent, Germany) in the wavelength range of 800−200 nm; fluorescence spectroscopy was performed by a fluorescence spectrophotometer (CARY ECLIPSE, Agilent, Germany) in the wavelength range of 800−200 nm; functional group testing was performed by a Fourier transform infrared (FTIR) spectrometer (Nicolet IS 50, Thermo Fisher, USA) in the wavenumber range of 4000−400 cm^{-1}. ^{1}H-NMR spectroscopy was performed by a nuclear magnetic resonance (NMR) spectrometer (AVANCE 400, Bruker, Germany). The tensile test of the dumbbell-shaped membranes (25 × 4 × 0.1 mm^3) was performed by a universal testing machine (ZQ-990A, China) with a gauge length of 10 mm and a crosshead speed of 10 mm/min, and five replicates were performed for each measurement to obtain the mechanical parameters. The thermal degradation process of the acrylate was evaluated by a thermogravimetric (TG) analysis device (STA2500, Netzsch, Germany) at a heating rate of 10 °C/min from room temperature to 600 °C in a nitrogen (N_2) atmosphere at a flow rate of 50 mL/min. The contact angle measurement was performed by a contact angle measuring instrument (DSA100E, KYUSS, Germany). The reflectance of composite membranes was measured by a UV−vis NIR spectrometer

https://doi.org/10.1021/acsomega.2c02162
ACS Omega 2022, 7, 25244−25252

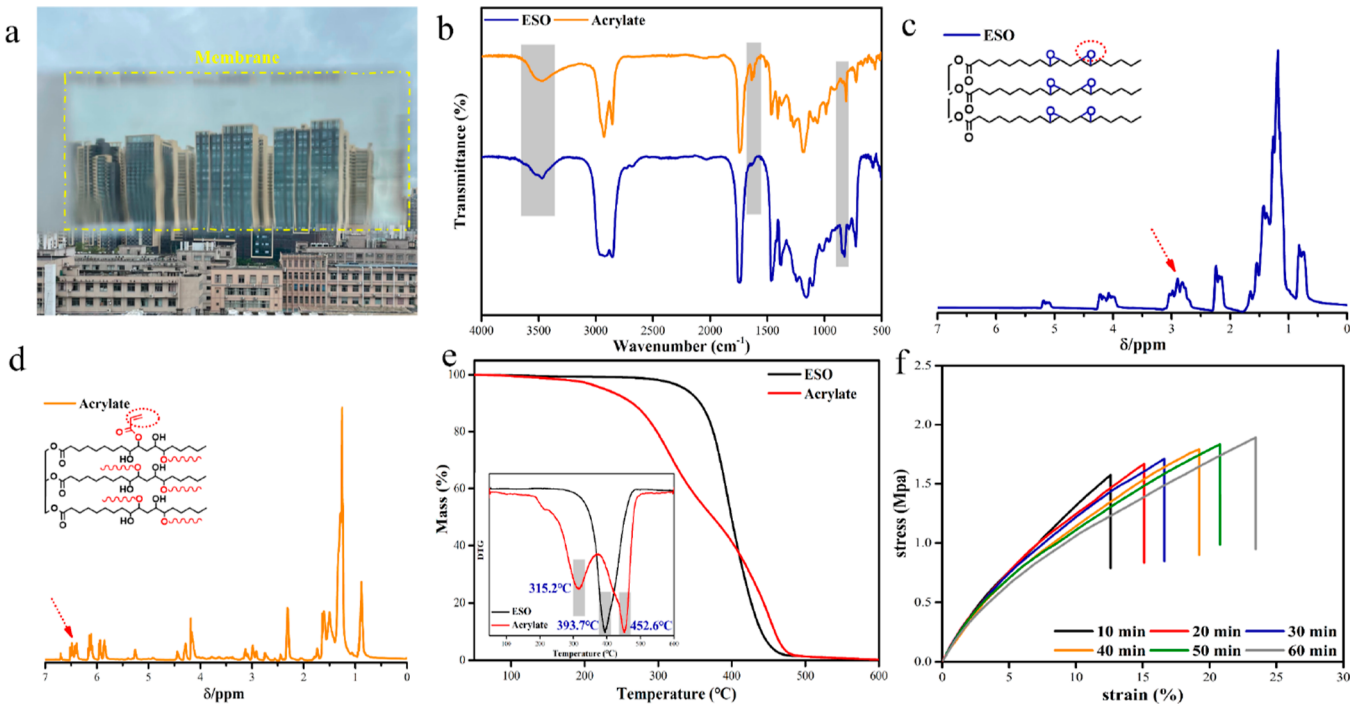

Figure 4. (a) Photo of an acrylate membrane. (b) FT-IR spectra of ESO and acrylate. (c) ^{1}H-NMR spectrum of ESO. (d) ^{1}H-NMR spectrum of acrylate. (e) TG curves of ESO and acrylate (illustration is DTG of ESO and acrylate). (f) Stress−strain curve of different curing times.

(UV-3600Plus, Shimadzu, Japan) and a near-infrared spectrum analyzer (TANGO-R, Bruker, Germany). The surface and elemental analyses of the composite membranes were measured by field emission scanning electron microscopy (SEM) (Sigma 300, Zeiss, Germany). The UV radiation test was performed by a UV illuminance meter (TM213, TENMARS, China)

RESULTS AND DISCUSSION

It was necessary to characterize the CDs. Using TEM, it was observed that the CDs show a sphere-like shape and possess good dispersion (Figure 3a). The electron transition and emission wavelengths of the CDs are confirmed by the UV absorption spectra and fluorescence spectra in Figure 3b. A sharp absorption peak appears at 215 nm, which may reflect the $\pi-\pi^*$ transition in the C═C domain of the carbon nucleus;[24] in addition, the absorption peak at 297 nm is attributed to the n$-\pi^*$ transition of the C═O bond.[25] The optimal emission wavelength of CDs is 542 nm, according to the fluorescence spectrum. As shown in the illustration in Figure 3b, the CDs exhibit good clarity under fluorescent light and emit bright green fluorescence under UV light (365 nm). To further understand the emission behavior of CDs, we excited CDs at 430−490 nm and found that the emission peaks of CDs did not depend on the excitation wavelength, indicating that CDs possess emission-independent excitation (EIE) properties (Figure 3c,d). Figure 3e shows the chemical structure of the CDs, with the absorption bands at 3354 and 3225 cm^{-1} attributed to the stretching vibrations of −OH and N−H, respectively.[26] In addition, the absorption band at 2925 cm^{-1} belongs to the stretching vibration of C−H.[27] The absorption bands at 1656 and 1605 cm^{-1} belong to C═O and C═C, respectively.[28] The appearance of absorption bands at 1112 and 1049 cm^{-1} is attributed to the asymmetric and symmetric stretching vibrations of C−O. FTIR results show that CDs have many reactive groups, which provide good water solubility. Finally, we explore the chemical bonds of CDs and their binding energies. Figure 3f shows the X-ray photoelectron spectroscopy (XPS) spectrum of the CDs, which shows three representative peaks of C 1s (285 eV), N 1s (400 eV), and O 1s (532 eV). The C 1s peak was decomposed into three peaks (Figure 3g): C═C (284 eV), C═O (285 eV), and HO−C═O (288 eV); the N1s peak was decomposed into two peaks (Figure 3h): pyridine nitrogen (398 eV) and pyrrole nitrogen (399 eV); and the O 1s peak was decomposed into three peaks (Figure 3i): C═O (530 eV), C−OH (531 eV), and C−O−C (532 eV). The XPS results show that the CDs contain many active chemical bonds, which are consistent with the FTIR results.

Figure 4a shows a picture of the acrylate membrane, which exhibits good transparency. To confirm the synthesis of the acrylate, FT-IR analysis and ^{1}H-NMR were performed. The FT-IR results are shown in Figure 4b, where ESO has an absorption band for the epoxy group at 822−842 cm^{-1},[29] and the acrylate does not show an absorption peak. In addition, the characteristic absorption bands of C═C and −OH at 1633 and 3450 cm^{-1} of acrylate confirm the successful synthesis of acrylate.[30,31] To further demonstrate the successful grafting of AA, we performed ^{1}H-NMR analysis, and the results are shown in Figure 4c,d. At δ = 3.10−2.80 ppm, the characteristic peak of hydrogen on the epoxy bond appeared in ESO,[32] while the characteristic peak of the epoxy bond in the acrylate weakened obviously. In addition, the peak at δ = 6.50−5.90 corresponds to the proton peak of acrylate (OOC−CH═CH$_2$), confirming the successful grafting of AA on ESO.[33] Figure 4e shows the TG curves of acrylate and ESO. It can be seen that the initial decomposition of ESO is at ∼300 °C, while that of acrylate is at ∼200 °C. ESO and acrylate are completely decomposed at 600 °C. From the results of DTG, it is observed that the degradation processes of ESO and acrylate are different: single

https://doi.org/10.1021/acsomega.2c02162
ACS Omega 2022, 7, 25244−25252

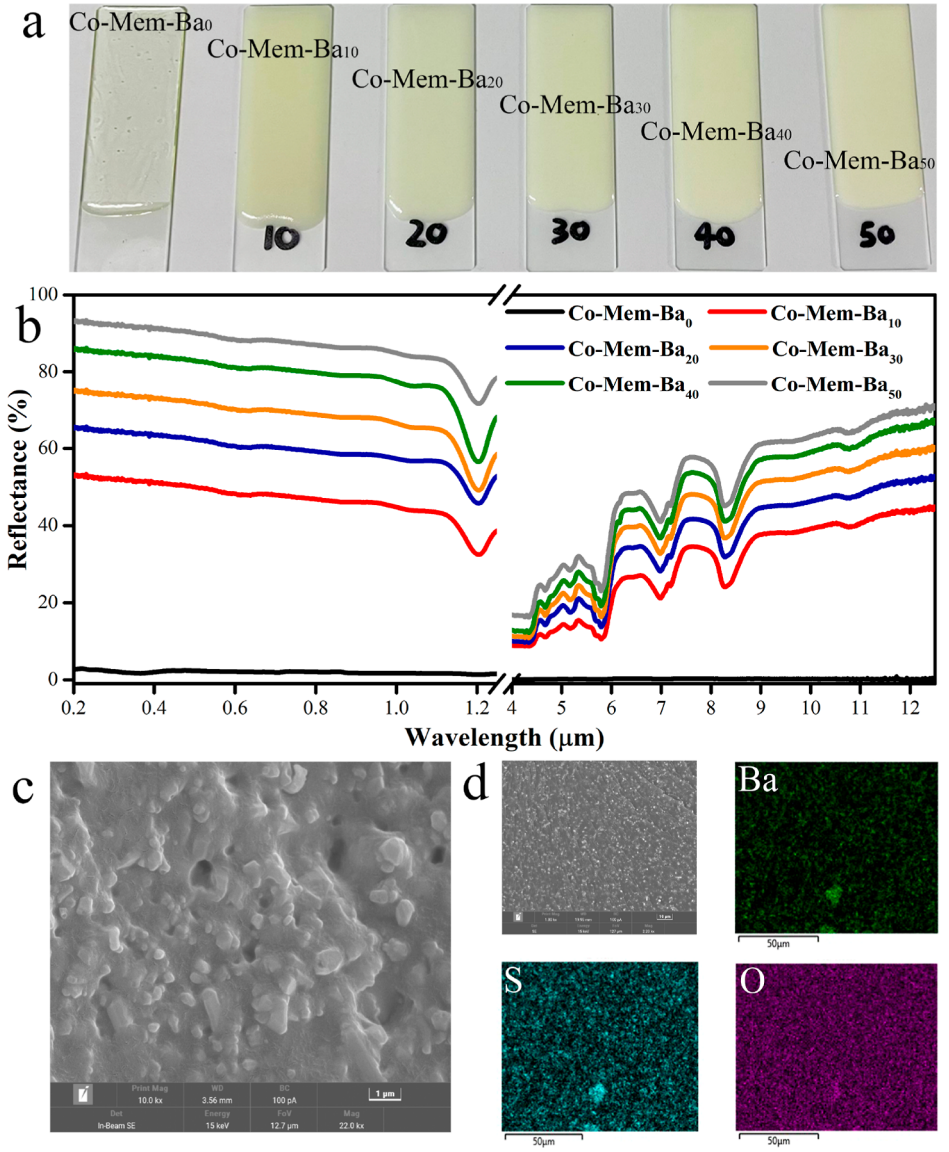

Figure 5. (a) Digital images of composite membranes; (b) reflectance of composite membranes (wavelength: 200−12,500 nm); (c) SEM image of Mem-Ba_{50} (scale: 1 μm); and (d) SEM−EDS images of Mem-Ba_{50}.

step for ESO and two steps for acrylate. The degradation of ESO involves the degradation and carbonization of the main chain, while the first step of acrylate degradation involves the degradation of branched chains, such as acrylate groups; the second step is degradation and carbonization of the main chain. Even though the initial decomposition of acrylate occurs at ∼200 °C, it can still meet the needs of applications in daily life, such as architectural coatings. Finally, we explored the effect of different curing times on the mechanical properties, and the results are shown in Figure 4f. As the curing time increases, the degree of cross-linking also increases, and the mechanical strength is significantly improved.

A series of digital images of the assembled composite membranes are shown in Figure 5a. The addition of high-whiteness particles has a significant whitening effect on the composite membrane. Figure S1 shows that the composite membrane has good flexibility. The first layer of the composite membrane consists of epoxy resin and CDs. Due to the existence of $\pi-\pi^*$ transition in CDs, it shows good absorption in the UV region and responds to excitation at UV wavelengths from 200 to 400 nm (Figure S2). The first layer serves two purposes: (1) it absorbs the UV light and converts it into visible light; (2) it protects the second layer which is responsible for providing the radiative cooling effect. In addition, CDs greatly limit their application due to their notorious AIQ effect.[34] Dispersing CDs in epoxy resins can better extend the service life of CDs while weakening the AIQ effect.[35,36] The second layer of composite membrane consists of acrylate and $BaSO_4$. In the study of UV-blocking materials, TiO_2 (3.2 eV) is the most commonly used,[37−39] and we chose $BaSO_4$ (∼6 eV) with a higher electronic band gap to reduce the absorption of UV radiation by the membrane. The long-term exposure of polymers to UV radiation tends to age and affects service life. The shift in UV absorption by CDs and the fact that $BaSO_4$ can reduce UV absorption are beneficial for the life of the membrane.

Figure 5b reflects the effect of $BaSO_4$ addition on the reflectance of the membranes at wavelengths 200−12500 nm. With the addition of $BaSO_4$, the reflectance of the membranes in the UV region increases, and when the addition of $BaSO_4$ is

https://doi.org/10.1021/acsomega.2c02162
ACS Omega 2022, 7, 25244−25252

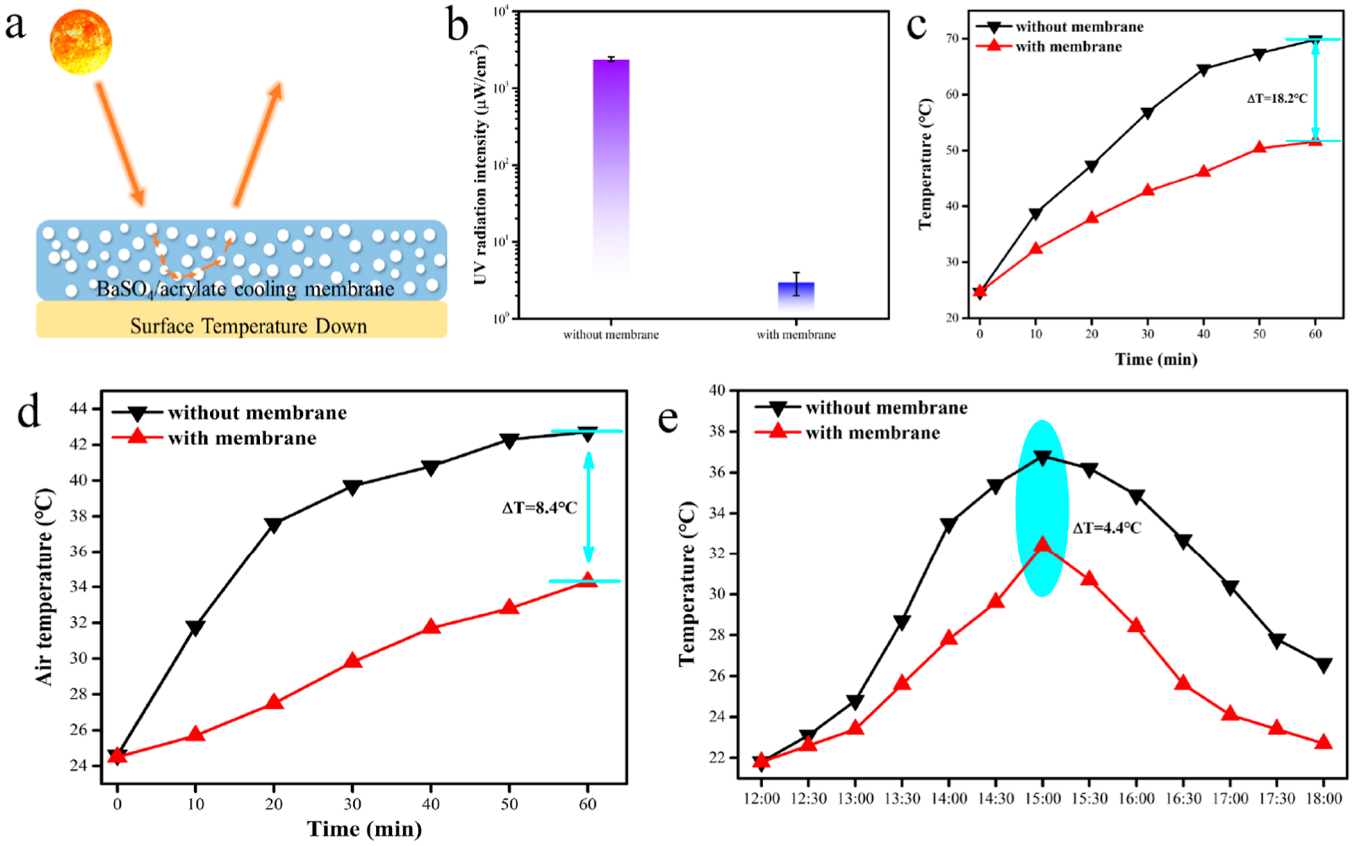

Figure 6. (a) Schematic diagram of a composite membrane reflecting infrared light. (b) UV-blocking ability of Co-Mem-Ba_{50}. (c) Co-Mem-Ba_{50} covered on the PMMA board, under the illumination of light; the surface temperature of the PMMA board without membrane and with membrane. (d) Air temperature inside the box (without membrane/with membrane, indoor test). (e) Air temperature inside the box (without membrane/with membrane, outdoor test).

50%, the reflectance reaches more than 90%. In addition, the reflectance of the membranes in the near-infrared region also increases with the increase of $BaSO_4$ content, which directly affects the radiative cooling performance of the membranes. The refraction of light needs to be performed in the voids in the membrane. Figure 5c shows the SEM image of the membrane, and the voids can be observed. In addition, Li et al.[10] concluded that the presence of voids in the membrane is beneficial for reflecting light. From the energy-dispersive system (EDS) images, it is clear that $BaSO_4$ is uniformly distributed, which is also favorable for radiative cooling (Figure 5d).

Figure 6a shows the principle of membrane reflecting infrared light. When sunlight shines on the membrane, the light is refracted several times by $BaSO_4$, which eventually reflects the infrared light, thus achieving a cooling effect. The UV-blocking performance of the composite membrane was tested outdoors, and the results are shown in Figure 6b, which show that the membrane blocks almost all UV light. To verify the radiative cooling performance of the membrane, the membrane was covered with a PMMA plate and heated under light. Figure 6c shows the change in the surface temperature of the PMMA plate with and without the membrane cover. The reflection of infrared light by the membrane slows down the rate of increase in surface temperature considerably, and after 60 min of heating, the membrane reduces the temperature by 18.2 °C. To further verify the radiative cooling performance of the composite membrane, a box was assembled using PMMA sheets to simulate a confined space, and radiative cooling tests were performed indoor (Figure S3a) and outdoor (Figure S3b), with the results shown in Figure 6d,e. In the indoor test, the air temperature inside the box was monitored at 10 min intervals, and the membrane could effectively reduce the temperature of the box after 60 min of heating; in the outdoor test, the temperature was monitored at 1 h intervals which reached a peak at 15 h with a temperature difference of 4.4 °C. The composite membrane effectively reduced the internal temperature and showed excellent radiative cooling performance.

The recycling of membranes is an important part of the sustainable use of material. Figure 7a shows the contact angles of different $BaSO_4$/acrylate membranes. $BaSO_4$ can effectively increase the contact angle of the membranes, and the increase of the contact angle can reduce the binding energy of the bonding surface and enable better separation between the membranes. Figure 7b shows the combination and separation of the composite membrane, and the improvement of the contact angle facilitates the separation and recovery of the membrane. We used tetrahydrofuran as the solvent to dissolve the $BaSO_4$/acrylate membrane. Next, after fully dissolving, solid−liquid separation is achieved using a centrifuge. After the solvent is completely volatilized, $BaSO_4$ can be recovered, and the acrylate can be reshaped into a membrane. Due to the volatilization of the solvent, there are many micropores in the recovered membrane, which will directly lead to the decline of the mechanical properties. The recovered solids and membrane were weighed, and the results showed that the recovery rate reached 95.90%.

https://doi.org/10.1021/acsomega.2c02162
ACS Omega 2022, 7, 25244−25252

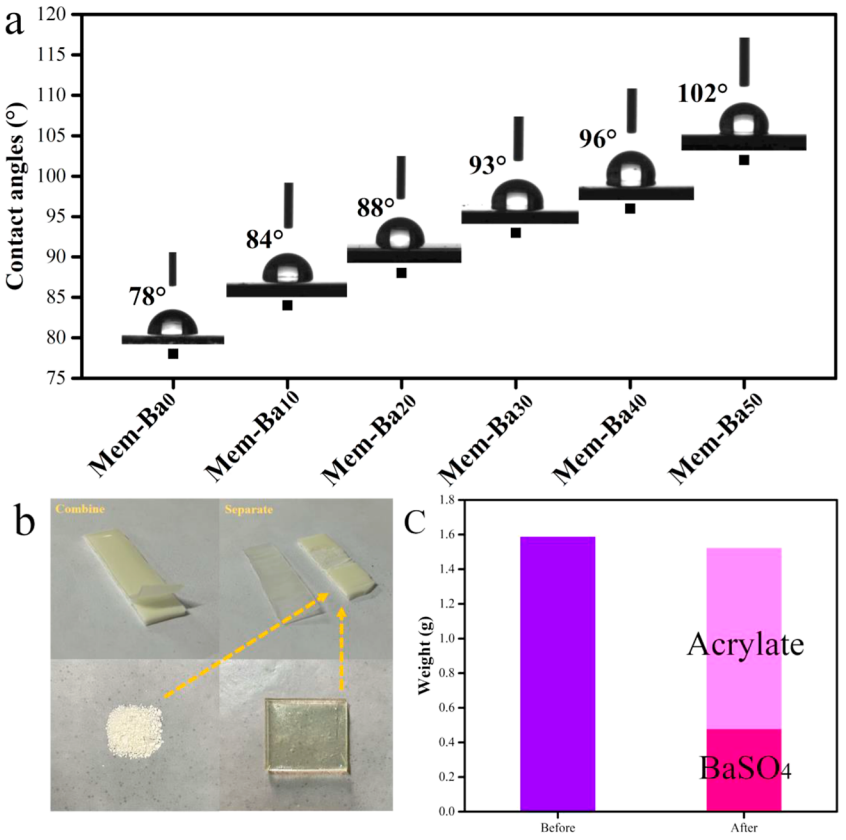

Figure 7. (a) Contact angles of different $BaSO_4$/acrylate membranes. (b) Separation of the composite membrane and recovery of Mem-Ba_{50}. (c) Mass change of Mem-Ba_{50} before and after separation.

CONCLUSIONS

In this work, we synthesized CDs and acrylates from xylose and ESO, respectively, and prepared composite membranes by a self-assembly strategy. The composite membrane exhibits excellent UV-blocking ability and almost shields against UV light with a shielding rate of 99%. In addition, the presence of $BaSO_4$ allows the membrane to reflect infrared light for a radiative cooling effect. The membrane achieved a cooling effect of 8.4 and 4.4 °C in indoor and outdoor tests, respectively. The first layer of the membrane composed of CDs and epoxy resin not only weakens UV rays but also reduces the absorption of UV rays by the second layer of the membrane, providing protection for it. The second membrane composed of $BaSO_4$ and acrylate mainly provides radiative cooling. Finally, we also discuss the recyclability of the $BaSO_4$/acrylate membrane, with a recovery of 95%, providing sustainable utilization of the membrane. In conclusion, the composite membrane exhibits excellent UV-blocking and radiative cooling properties and is expected to be popularized and used in low latitudes or areas close to the equator.

ASSOCIATED CONTENT

Supporting Information

The Supporting Information is available free of charge at https://pubs.acs.org/doi/10.1021/acsomega.2c02162.

Digital image of Co-Mem-Ba_{50}, CDs excited by wavelengths (200−400 nm), and schematic diagram of the radiative cooling performance test (PDF)

AUTHOR INFORMATION

Corresponding Author

Wei Gao − *School of Resources, Environment and Materials, Guangxi University, Nanning, Guangxi 530004, China; Guangxi Engineering and Technology Research Center for High Quality Structural Panels from Biomass Wastes, Nanning, Guangxi 530004, China;* orcid.org/0000-0002-4353-6599; Email: galaxy@gxu.edu.cn

Authors

Shaofeng Liang − *School of Resources, Environment and Materials, Guangxi University, Nanning, Guangxi 530004, China*

Muqun Wang − *School of Resources, Environment and Materials, Guangxi University, Nanning, Guangxi 530004, China*

Hailin Diao − *Forestry College, Guangxi University, Nanning, Guangxi 530004, China*

Jianju Luo − *School of Resources, Environment and Materials, Guangxi University, Nanning, Guangxi 530004, China*

Complete contact information is available at: https://pubs.acs.org/10.1021/acsomega.2c02162

Author Contributions

All the photos in figures were taken by S.L., and this paper was written with contributions from all authors. All authors have given their approval to the final version of the paper. S.L.: methodology, visualization, software, and writing−−original draft; M.W.: investigation, methodology, visualization, and writing−−original draft; H.D.: software and resources; J.L.:

https://doi.org/10.1021/acsomega.2c02162
ACS Omega 2022, 7, 25244−25252

software and resources; and W.G.: resources, writing review and editing, and funding acquisition.

Notes

The authors declare no competing financial interest.

■ ACKNOWLEDGMENTS

This research was funded by the Key R&D projects in Guangxi (AB21196033) and by the Chongzuo science and technology planning project (FA2017005).

■ REFERENCES

(1) Chen, M.; Pang, D.; Mandal, J.; Chen, X.; Yan, H.; He, Y.; Yu, N.; Yang, Y. Designing Mesoporous Photonic Structures for High-Performance Passive Daytime Radiative Cooling. *Nano Lett.* **2021**, *21*, 1412−1418.

(2) Gentle, A. R.; Smith, G. B. Radiative Heat Pumping from the Earth Using Surface Phonon Resonant Nanoparticles. *Nano Lett.* **2010**, *10*, 373−379.

(3) Zhou, L.; Song, H.; Liang, J.; Singer, M.; Zhou, M.; Stegenburgs, E.; Zhang, N.; Xu, C.; Ng, T.; Yu, Z.; Ooi, B.; Gan, Q. A polydimethylsiloxane-coated metal structure for all-day radiative cooling. *Nat. Sustain.* **2019**, *2*, 718−724.

(4) Gao, Y.; Song, X.; Farooq, A. S.; Zhang, P. Cooling performance of porous polymer radiative coating under different environmental conditions throughout all-year. *Sol. Energy* **2021**, *228*, 474−485.

(5) Baniassadi, A.; Sailor, D. J.; Ban-Weiss, G. A. Potential energy and climate benefits of super-cool materials as a rooftop strategy. *Urban Clim.* **2019**, *29*, 100495.

(6) Zeyghami, M.; Goswami, D. Y.; Stefanakos, E. A review of clear sky radiative cooling developments and applications in renewable power systems and passive building cooling. *Sol. Energy Mater. Sol. Cells* **2018**, *178*, 115−128.

(7) Bao, H.; Yan, C.; Wang, B.; Fang, X.; Zhao, C. Y.; Ruan, X. Double-layer nanoparticle-based coatings for efficient terrestrial radiative cooling. *Sol. Energy Mater. Sol. Cells* **2017**, *168*, 78−84.

(8) Cheng, Z.; Han, H.; Wang, F.; Yan, Y.; Shi, X.; Liang, H.; Zhang, X.; Shuai, Y. Efficient radiative cooling coating with biomimetic human skin wrinkle structure. *Nano Energy* **2021**, *89*, 106377.

(9) Mandal, J.; Fu, Y.; Overvig, A. C.; Jia, M.; Sun, K.; Shi, N. N.; Zhou, H.; Xiao, X.; Yu, N.; Yang, Y. Hierarchically porous polymer coatings for highly efficient passive daytime radiative cooling. *Science* **2018**, *362*, 315−319.

(10) Li, X.; Peoples, J.; Yao, P.; Ruan, X. Ultrawhite $BaSO_4$ Paints and Films for Remarkable Daytime Subambient Radiative Cooling. *ACS Appl. Mater. Interfaces* **2021**, *13*, 21733−21739.

(11) Li, X.; Peoples, J.; Huang, Z.; Zhao, Z.; Qiu, J.; Ruan, X. Full Daytime Sub-ambient Radiative Cooling in Commercial-like Paints with High Figure of Merit. *Cell Rep. Phys. Sci.* **2020**, *1*, 100221.

(12) Tremblay-Parrado, K.-K.; García-Astrain, C.; Avérous, L. Click chemistry for the synthesis of biobased polymers and networks derived from vegetable oils. *Green Chem.* **2021**, *23*, 4296−4327.

(13) Cheng, Q.-Y.; An, X.-P.; Li, Y.-D.; Huang, C.-L.; Zeng, J.-B. Sustainable and Biodegradable Superhydrophobic Coating from Epoxidized Soybean Oil and ZnO Nanoparticles on Cellulosic Substrates for Efficient Oil/Water Separation. *ACS Sustain. Chem. Eng.* **2017**, *5*, 11440−11450.

(14) Wu, Q.; Hu, Y.; Tang, J.; Zhang, J.; Wang, C.; Shang, Q.; Feng, G.; Liu, C.; Zhou, Y.; Lei, W. High-Performance Soybean-Oil-Based Epoxy Acrylate Resins: "Green" Synthesis and Application in UV-Curable Coatings. *ACS Sustain. Chem. Eng.* **2018**, *6*, 8340−8349.

(15) von der Gathen, P.; Kivi, R.; Wohltmann, I.; Salawitch, R. J.; Rex, M. Climate change favours large seasonal loss of Arctic ozone. *Nat. Commun.* **2021**, *12*, 3886.

(16) Kerr, R. A. New Assaults Seen on Earth's Ozone Shield. *Science* **1992**, *255*, 797−798.

(17) Uthirakumar, P.; Devendiran, M.; Yun, J.-H.; Kim, G. C.; Kalaiarasan, S.; Lee, I.-H. Role of carbon quantum dots and film thickness on enhanced UV shielding capability of flexible polymer film containing carbon quantum dots/N-doped ZnO nanoparticles. *Opt. Mater.* **2018**, *84*, 771−777.

(18) Periyayya, U.; S, M.; Khan, R.; Dao, V.-D.; Tran, V.-H.; Lee, I.-H. Carbon quantum dots decorated leaf-like CuO nanosheets and their improved dispersion for an excellent UV-shielding properties in polymer films. *RSC Adv.* **2015**, *5*, 71968−71972.

(19) Barman, B. K.; Handegård, Ø. S.; Hernández-Pinilla, D.; Shinde, S. L.; Nagao, T. Transparent Hard Coatings with SiON-Encapsulated N-Doped Carbon Dots for Complete UV Blocking and White Light Emission. *ACS Appl. Electron. Mater.* **2021**, *3*, 3761−3773.

(20) Yang, P.; Zhu, Z.; Zhang, T.; Chen, M.; Cao, Y.; Zhang, W.; Wang, X.; Zhou, X.; Chen, W. Facile synthesis and photo-luminescence mechanism of green emitting xylose-derived carbon dots for anti-counterfeit printing. *Carbon* **2019**, *146*, 636−649.

(21) Feng, Z.; Adolfsson, K. H.; Xu, Y.; Fang, H.; Hakkarainen, M.; Wu, M. Carbon dot/polymer nanocomposites: From green synthesis to energy, environmental and biomedical applications. *Sustainable Mater. Technol.* **2021**, *29*, No. e00304.

(22) Shauloff, N.; Bhattacharya, S.; Jelinek, R. Elastic carbon dot/polymer films for fluorescent tensile sensing and mechano-optical tuning. *Carbon* **2019**, *152*, 363−371.

(23) De, B.; Kumar, M.; Mandal, B. B.; Karak, N. An in situ prepared photo-luminescent transparent biocompatible hyperbranched epoxy/carbon dot nanocomposite. *RSC Adv.* **2015**, *5*, 74692−74704.

(24) Singh, J.; Kaur, S.; Lee, J.; Mehta, A.; Kumar, S.; Kim, K.-H.; Basu, S.; Rawat, M. Highly fluorescent carbon dots derived from Mangifera indica leaves for selective detection of metal ions. *Sci. Total Environ.* **2020**, *720*, 137604.

(25) Qu, D.; Zheng, M.; Du, P.; Zhou, Y.; Zhang, L.; Li, D.; Tan, H.; Zhao, Z.; Xie, Z.; Sun, Z. Highly luminescent S, N co-doped graphene quantum dots with broad visible absorption bands for visible light photocatalysts. *Nanoscale* **2013**, *5*, 12272−12277.

(26) Eskalen, H.; Uruş, S.; Cömertpay, S.; Kurt, A. H.; Özgan, Ş. Microwave-assisted ultra-fast synthesis of carbon quantum dots from linter: Fluorescence cancer imaging and human cell growth inhibition properties. *Ind. Crops Prod.* **2020**, *147*, 112209.

(27) Zhu, S.; Song, Y.; Zhao, X.; Shao, J.; Zhang, J.; Bai, Y. The photoluminescence mechanism in carbon dots (graphene quantum dots, carbon nanodots, and polymer dots): current state and future perspective. *Nano Res.* **2015**, *8*, 355−381.

(28) Wang, C.; Xu, Z.; Cheng, H.; Lin, H.; Mark, G. A hydrothermal route to water-stable luminescent carbon dots as nanosensors for pH and temperature. *Carbon* **2015**, *82*, 87−95.

(29) Karadeniz, K.; Alkolu, Y.; Sen, M. Y. A novel polyurethanes from epoxidized soybean oil synthesized by ring opening with bifunctional compounds. *Polym. Bull.* **2016**, *74*, 1−21.

(30) Aung, M. M.; Yaakob, Z.; Abdullah, L. C. A comparative study of acrylate oligomer on Jatropha and Palm oil-based UV-curable surface coating. *Ind. Crop. Prod.* **2015**, *77*, 1047−1052.

(31) Patil, C. K.; Rajput, S. D.; Marathe, R. J.; Kulkarni, R. D.; Phadnis, H.; Sohn, D.; Mahulikar, P. P.; Gite, V. V. Synthesis of bio-based polyurethane coatings from vegetable oil and dicarboxylic acids. *Prog. Org. Coat.* **2017**, *106*, 87−95.

(32) Zhang, C.; Ding, R.; Kessler, M. R. Reduction of Epoxidized Vegetable Oils: A Novel Method to Prepare Bio-Based Polyols for Polyurethanes. *Macromol. Rapid Commun.* **2014**, *35*, 1068−1074.

(33) Wong, J. L.; Aung, M. M.; Lim, H. N.; Jamil, S. Spectroscopic Analysis of Epoxidised Jatropha Oil (EJO) and Acrylated Epoxidised Jatropha Oil (AEJO). *Pertanika J. Trop. Agric. Sci.* **2017**, *40*, 435−447.

(34) Xia, C.; Zhu, S.; Feng, T.; Yang, M.; Yang, B. Evolution and Synthesis of Carbon Dots: From Carbon Dots to Carbonized Polymer Dots. *Adv. Sci.* **2019**, *6*, 1901316.

(35) Liu, Y.; Wang, P.; Fernando, K. A. S.; LeCroy, G. E.; Maimaiti, H.; Harruff-Miller, B. A.; Lewis, W. K.; Bunker, C. E.; Hou, Z.-L.; Sun, Y.-P. Enhanced Fluorescence Properties of Carbon Dots in Polymer Films. *J. Mater. Chem. C* **2016**, *4*, 6967−6974.

https://doi.org/10.1021/acsomega.2c02162
ACS Omega 2022, 7, 25244−25252

(36) Lee, U.; Heo, E.; Le, T.-H.; Lee, H.; Kim, S.; Lee, S.; Jo, H.; Yoon, H. Carbon dots for epoxy curing: Anti-forgery patterns with long-term luminescent stability. *Chem. Eng. J.* **2021**, *405*, 126988.
(37) Zhang, Y.; Yu, L.; Shen, S.; Meng, X. TiO_2/SiO_2 hybrid nanomaterials: synthesis and variable UV-blocking properties. *J. Sol-Gel Sci. Technol.* **2011**, *58*, 326−329.
(38) Kwon, H.-J.; Lee, Y.-W.; Kim, H.-S.; Zhoh, C.-K.; Park, K.-W. One-dimensional TiO_2 nanostructures with improved UV-blocking properties. *Mater. Lett.* **2013**, *93*, 175−178.
(39) Zheng, W.; Dong, Y.; Li, T.; Chen, J.; Chen, X.; Dai, Y.; He, G. MgO blocking layer induced highly UV responsive TiO_2 nanoparticles based self-powered photodetectors. *J. Alloys Compd.* **2021**, *869*, 159299.

https://doi.org/10.1021/acsomega.2c02162
ACS Omega 2022, 7, 25244−25252